Published in final edited form as:
J Mol Biol. 2008 November 7; 383(2): 367–379. doi:10.1016/j.jmb.2008.08.011.

Crystal structure of *Escherichia coli* Rnk, a new RNA polymerase-interacting protein

Valerie Lamour[1], **Steven T. Rutherford**[2], **Konstantin Kuznedelov**[3], **Udupi A. Ramagopal**[4], **Richard L. Gourse**[2], **Konstantin Severinov**[3], and **Seth A. Darst**[1,*]

1*The Rockefeller University, Laboratory of Molecular Biophysics, 1230 York Avenue, New York, NY 10021*

2*University of Wisconsin-Madison, Dept. of Bacteriology, 1550 Linden Drive, Madison, WI 53706*

3*Waksman Institute, Dept. of Molecular Biology and Biochemistry, Rutgers University, Piscataway, NJ 08854*

4*Albert Einstein College of Medicine, Dept. of Biochemistry, 1300 Morris Park Avenue, Bronx, NY 10461*

Abstract

Sequence-based searches identified a new family of genes in proteobacteria, named *rnk*, that shares high sequence similarity with the C-terminal domains of the Gre-factors (GreA, GreB) and the *Thermus/Deinococcus* anti-Gre-factor Gfh1. We solved the X-ray crystal structure of *Escherichia coli* Rnk at 1.9 Å-resolution using the anomalous signal from the native protein. The Rnk structure strikingly resembles those of *E. coli* GreA, GreB, and *Thermus* Gfh1, all of which are RNAP secondary channel effectors, and all of which have a C-terminal domain belonging to the FKBP fold. Rnk, however, has a much shorter N-terminal coiled-coil. Rnk does not stimulate transcript cleavage *in vitro*, nor does it reduce the lifetime of the complex formed by RNAP on promoters. We show that Rnk competes with the Gre-factors and DksA (another RNAP secondary channel effector) for binding to RNAP *in vitro*, and although we found that the concentration of Rnk *in vivo* was much lower than that of DksA, it was similar to that of GreB, consistent with a potential regulatory role for Rnk as an anti-Gre factor.

Introduction

Gre-factors (GreA and GreB) [1] promote transcription elongation in bacteria by stimulating the intrinsic endonucleolytic transcript cleavage activity of the RNA polymerase (RNAP) [2]. Gre-factors are required for the natural progression of RNAP *in vivo* [3; 4]. In addition to rescuing arrested complexes and increasing the overall elongation rate [5], Gre factors may play a role in modulating RNAP behavior at pause signals [3], increasing transcriptional fidelity [6], and in stimulating promoter clearance [7; 8; 9].

Gre factors comprise two structural/functional domains [10]. The N-terminal domain (NTD) consists of a 60 Å-long coiled-coil that extends into the RNAP secondary channel to the RNAP catalytic site and is critical for stimulating transcript cleavage activity [11; 12; 13]. The globular C-terminal domain (CTD) consists of a β-sheet flanked by a small α-helix [10; 11; 12]. The CTD,

*Corresponding author: Phone: 212-327-7479; Fax: 212-327-7477; e-mail: darst@rockefeller.edu.

Accession Numbers
Coordinates and structure factors have been deposited in the Protein Data Bank with accession number 3BMB.

which is important for binding RNAP, interacts with the β' subunit of RNAP at the entrance of the RNAP secondary channel [10; 11; 12; 13]. Biochemical and structural data have converged to a model whereby conserved acidic residues at the Gre coiled-coil tip stabilize the binding of the second Mg^{2+}-ion in the RNAP active site required for the endonucleolytic cleavage reaction [13; 14; 15; 16].

Similar to the Gre-factors, DksA is organized into two structural domains. It has a long coiled-coil similar in structure to that of the Gre-factors, but its second domain is distinct and contains a Zn-finger motif [17]. Like the Gre-factors, DksA binds to RNAP with its coiled-coil structural element placed directly in the RNAP secondary channel ([17; 18]; I. Toulokhonov, R.L.G., unpublished data). DksA is essential for control of rRNA promoters at all times in bacterial growth, including following nutrient starvation, when it cooperates with the alarmone ppGpp to regulate expression from many operons during the stringent response [19; 20]. Recent studies have shown that GreB can fulfill some roles of DksA *in vitro*, allowing rRNA promoters to sense changes in the concentrations of ppGpp and the first NTP in the transcript when the *dksA* gene is deleted [21].

In addition to a GreA homolog, the hyperthermophiles *Thermus thermophilus (Tth)* and *Thermus aquaticus (Taq)* possess another Gre-factor homolog, Gfh1, that lacks transcript cleavage activity and competes with GreA for RNAP binding [22]. This anti-Gre factor contains domains structurally similar to GreA [10; 23; 24; 25]. Crystal structures of *Taq* and *Tth* Gfh1 revealed a large conformational change compared with *Escherichia coli (Ec)* GreA, affecting the relative orientation of the coiled-coil and the C-terminal domains. Biochemical data suggested that Gfh1 binds RNAP in a conformation similar to that observed for the Gre-factors, but that it switches to an alternate conformation at high pH [10; 13; 25]. Conserved inter-domain contacts that may stabilize the GreA-like conformation of Gfh1 were revealed by modeling Gfh1 in its GreA-like conformation [23].

Our database searches for Gre-factor/Gfh1 homologs revealed another family of proteins in proteobacteria, known as *regulator of nucleoside kinase* (Rnk), that shares substantial sequence similarity with the Gre and anti-Gre factors. Mutations in *rnk* drastically reduce the level of nucleoside diphosphate kinase (Ndk) in *Ec*, which is an important enzyme involved in maintaining cellular NTP and dNTP pools [26]. By an unknown mechanism, *Ec* Rnk is also a multicopy suppressor of an alginate-deficient phenotype in *Pseudomonas aeruginosa* caused by deletion of *algQ* (also called *algR2*; [27]).

We present here the 1.9 Å-resolution crystal structure of *Ec* Rnk. The structure reveals a globular CTD that is structurally conserved with the Gre and anti-Gre factors, but an NTD containing a much shorter coiled-coil. The CTD belongs to the FKBP fold first identified in the immunophilin family [28]. The FKBP fold has been found in proteins with a wide variety of functions, from a peptidyl-prolyl isomerase to proteins that make protein/protein interactions within large molecular assemblies. Structural features of the Gre/Gfh1/Rnk FKBP domain show that it belongs to the latter group. We further demonstrate that *Ec* Rnk competes for binding and function with the RNAP secondary channel effectors GreA, GreB, and DksA *in vitro*. Unlike Gre-factors [10; 11], however, Rnk does not crosslink with the 3'-end of the RNA transcript in the RNAP ternary elongation complex (TEC), stimulate transcript cleavage, or decrease the lifetime of the RNAP-promoter complex [21]. The cellular concentration of Rnk in both log and stationary phase is comparable to that of GreB, and only a few-fold lower than GreA, suggesting that Rnk might compete with, and thereby regulate, Gre factor activity *in vivo*. We found that Rnk is dispensable for regulation of rRNA transcription initiation *in vivo*, consistent with its much lower cellular concentration than DksA. However, we also were unable to detect effects of Rnk on Gre factor function in transcription from the *tnaC* promoter

in vivo. Our results thereby suggest a tantalizing, although unconfirmed, role for Rnk *in vivo* as an anti-Gre factor.

Results

Identification of Rnk proteins as a new family of Gre factor homologs

The anti-Gre factor Gfh1 has only been found in the *Thermus/Deinoccocus* phylum. Searching for Gfh1 homologs using the program Ballast [29], we found proteins sharing significant sequence similarity in a region covering the CTD (residues 79 to 151) of *Taq* Gfh1. The Gfh1 homologs belong to the nucleoside diphosphate kinase regulator family (Rnk), with the closest homolog from *Geobacter sulfurreducens* (expectation value 1×10^{-9}). In an inverse search using *Ec* Rnk, elongation factors were found immediately after Rnk family members (elongation factor Q82T10_niteu : expectation value 1×10^{-28}, ballast rank 11, blast rank 19).

During our search, we found that the Rnk proteins seem to be limited to gram negative proteobacteria (Figure S1). *Ec* Rnk (sw:P40679) is a 136 amino acid protein that shares significant sequence identity with *Taq* Gfh1: 22.79% identity between the full length proteins, and 28.9% identity over their CTDs (*Ec* Rnk residues 48 to 136, *Taq* Gfh1 residues 79 to the C-terminus). By comparison, *Ec* Rnk shares 22.06% sequence identity with *Ec* GreA and 15.44% with *Ec* GreB (Gfh1 shares 25 % identity with *Ec* GreA). The N-terminal residues of Rnk (residues 1 to 47) do not exhibit significant sequence similarity with the Gre-factor NTDs (residues 1 to 76).

Secondary structure prediction for Rnk using PHD [30] revealed that the CTD of Rnk possesses secondary structure elements similar to the Gre and anti-Gre factors. The secondary structure elements for the Rnk NTD are also predicted to be similar to the Gre factors, but the coiled-coil helices are much shorter (Figure 1A).

Ec Rnk structure

The purified, native *Ec* Rnk protein was crystallized by hanging-drop vapor diffusion. The crystals diffracted beyond 1.9 Å-resolution and were also very resistant to radiation damage. This allowed us to collect a highly redundant dataset with relatively low energy X-rays (1.74 Å wavelength; Table 1) to facilitate detection of the sulfur anomalous signal directly from the native protein. The asymmetric unit contains two Rnk molecules as well as 10 sulfate and 2 chloride ions (Figure S2A). The chloride ions bind in a small hydrophobic pocket of the protein, whereas the sulfate ions bind to arginine residues on the surface of the protein, with two of them sitting between the two molecules in the asymmetric unit. The overall structural organization of Rnk is similar to the Gre-factors (Figure 1B), with an N-terminal coiled-coil and a C-terminal globular domain. As expected from the sequence similarity, the C-terminal globular domain superimposes closely on that of the Gre factors. The CTDs of *Ec* Rnk and *Ec* GreA superimpose with a root-mean-square-deviation (rmsd) of 1.96 Å over 68 Cα positions. The CTDs of *Ec* Rnk and *Taq* Gfh1 superimpose with an rmsd of 4.1 Å over 54 Cα positions, a larger value due to conformational variations in flexible loops connecting the secondary structural elements. The N-terminal coiled-coil of Rnk is about 22 Å shorter than the Gre or Gfh1 coiled-coil (Figure 2A).

Comparison of the *Ec* GreA, *Taq* Gfh1, and *Ec* Rnk structures, all aligned by their C-terminal domains, reveals three different orientations of the N-terminal coiled-coil domains with respect to the CTDs. The Rnk NTD is rotated 104° with respect to the GreA NTD, while the Gfh1 NTD is rotated 178° [23] (Figure 2A). The *Ec* Rnk NTD is maintained against its CTD by a hydrogen bond network involving the side chains of Asn9 and Asp12 from the NTD, and Thr55, Tyr77, and Glu129 from the CTD (Figure 2B). Several residues are also engaged in main chain/

main chain interactions, and the side chain of Arg3 in the N-terminal arm of the protein interacts with the carbonyl group of Leu99 in the CTD. Additional hydrophobic interactions at the interface between the two domains of the protein stabilize the overall conformation.

Structural homology with the FKBP domain

While the NTD is variable at the sequence and structural level between the Gre and Rnk families, the CTD is well conserved even when comparing distant species. Proteins with the closest structural similarity to the Rnk CTD, identified from a search using DALI (http://www.ebi.ac.uk/dali), aside from the Gre factors (*Ec* GreA, Z=11.0, PDB entry PDB: 1GRJ), are proteins belonging to the FKBP fold: the FK506-binding proteins FKBP51 (Z=6.0, PDB:1KT0) and FKBP12 (Z=5.8, PDB:1FKJ), Rv2118c, a methyltransferase from mycobacterium (Z=5.3, 1I9G), a domain of the Trigger factor (Z=4.7, PDB:1HXV), a prolylisomerase Mip (Z=4.9, PDB:1FD9), and SurA, a molecular chaperone (Z=3.8, PDB: 1M5Y).

The commonality among all these proteins is a core structure comprising an antiparallel β-sheet wrapped around a central α-helix of two-turns. The number of β-strands in the FKBP β-sheet can vary from 4 for Rv2118c, SurA, and the Trigger factor, to 5 for FKBP51, FKBP12, Mip, and the Gre factors (where the N-terminal arm of the protein is considered part of the C-terminal β-sheet). Depending on the protein, the β-sheet can adopt slightly different spatial orientations relative to the α-helix. This structural relationship between the *Ec* GreA CTD and the FKBP domain was previously mentioned in the structural study of *h*par14 [31], a parvulin-like human peptidyl-prolyl isomerase (Dali score with Rnk CTD Z=2.4, PDB:1EQ3).

Initially, FKBP domains were named for their ability to bind the immunosuppressive drug FK506 [28]. The domain is found associated with a variety of protein functions. Some display peptidyl-prolyl *cis/trans* isomerase activity (PPIase), like FKBP12 [32], the Trigger factor [33], and Mip [34], while some have evolved into protein/protein interaction domains, like the Rv2118c methyltransferase [35], and one of the FKPB domains in FKBP51 [36] and SurA [37].

FKBP proteins that display PPIase activity present a hollow surface that leads into the core of the structure to the N-terminal part of the central α-helix. This cavity is surrounded by conserved residues that are able to bind oligopeptide substrates, and in some cases the inhibitor FK506 (Figure S3A). The Trigger factor, although possessing weak PPiase activity, does not bind FK506 due to subtle structural changes that lead to steric hindrance [33]. In contrast, FKBP proteins without PPIase activity do not show significant sequence homology with the PPIase family, and the cavity is either filled by loops (Figure S3B) or flattened like in the Gre factors, exposing the N-terminal end of the core α-helix (Figure S3A). Gre factors share no significant sequence similarity with most PPIases. Together with divergent Gre factor sequences, however, weak sequence similarity can be detected with the Trigger factor from *D. radiodurans* (TIG_deira) in a PSI-BLAST search [38] after the first iteration (score 0.91) in the C-terminal FKBP domain (from *Ec* Rnk residue 58 to 120).

Rnk competes with transcription factors that bind near the RNAP secondary channel *in vitro*

The sequence (Figure 1A) and structural (Figure 2A) similarity of Rnk with the Gre-factors and Gfh1, which bind RNAP at the entry to the secondary channel [13], suggest that Rnk may also interact with RNAP in a similar manner. Therefore, we tested directly whether Rnk interacts with RNAP. Immobilized hexa-histidine-tagged (His_6)-Rnk clearly co-immobilized *Ec* core RNAP (Figure 3A, lane 4), while RNAP alone was not detectably retained on the column (Figure 3A, lane 8), confirming an Rnk/RNAP protein/protein interaction. Native polyacrylamide gel electrophoresis analysis also indicated Rnk binding to RNAP (data not shown).

If Rnk binds RNAP at the entrance to the RNAP secondary channel, as suggested by the sequence and structural similarity with Gre-factors and Gfh1, then Rnk should bind RNAP competitively with Gre-factors. It has been previously shown that GreA and GreB interact, or are in close proximity to, the RNA transcript 3'-end since the Gre-factors crosslink to probes incorporated into the RNA 3'-end in TECs (Figure 3B, lane 3; [10; 11]. The RNA does not crosslink to Rnk (Figure 3B, lane 2), presumably because the short coiled-coil of Rnk is unable to enter the RNAP secondary channel and reach the 3'-end of the RNA transcript. Addition of Rnk reduces the efficiency of RNA crosslinking to GreA, indicating that Rnk binding to RNAP displaces GreA in a competitive manner (Fig. 3B, lanes 4–6). The results of additional experiments (native gel electrophoresis, data not shown; gel filtration experiments, Figure S4) corroborate the conclusion that Rnk and Gre-factor binding to RNAP is mutually exclusive. Although Rnk exhibits sequence (Figure 1A), structural (Figure 2A), and functional (competitive binding) similarity with the Gre-factors, Rnk, in contrast to the Gre-factors, does not stimulate transcript cleavage in TECs containing either 6-mer or 9-mer RNA transcripts (Figure 3C).

Finally, using a filter-binding assay, we tested whether Rnk reduced the lifetime of the RNAP-promoter complex in a manner similar to DksA and the Gre factors (Figure 4). DksA, GreB, and GreA each decreased the absolute half-life of the competitor-resistant complex formed between RNAP and promoter DNA (compare absolute half-lives of the complexes formed by RNAP in the absence of factor with those in the presence of DksA, GreB, and GreA) [20; 21; 39]. In contrast, Rnk had no effect on the half-life of the complex (Figure 4A).

We also tested whether Rnk would alter the effects of DksA and the Gre factors on promoter complex lifetime. Whereas DksA or GreB alone decreased the lifetime of the complex ~10-fold (from 53 min to 5–7 min), an equimolar concentration of Rnk either partially reduced (DksA) or eliminated (GreB) the effect of the factor on half-life (Figure 4B, 4C). As reported previously [21], more GreA than DksA or GreB was required to reduce the lifetime of the promoter complex, and the decrease caused by GreA was smaller than that caused by GreB or DksA (Figure 4D), suggesting that GreA binds to the promoter complex with lower affinity than GreB or DksA. Not surprisingly, Rnk, even at less than equimolar concentrations, essentially eliminated the effect of GreA on promoter lifetime (Figure 4D). We conclude that Rnk can compete with DksA and the Gre factors for binding to the promoter complex *in vitro*.

Rnk likely is dispensable for rRNA and *tnaC* regulation *in vivo*

The competitive effects observed at comparable concentrations of Rnk, DksA, and Gre factors *in vitro* would only affect promoter complexes *in vivo* if the concentrations of the factors were also comparable as were solution conditions and macromolecular crowding. Therefore, we measured Rnk, DksA, GreA, and GreB levels in cell lysates using Western blots. The Rnk concentration was ~9-fold lower than that of DksA in log phase and ~6-fold lower in stationary phase (Figure 5A). Since an equal concentration of Rnk was insufficient to completely compete away DksA function *in vitro* (suggesting the concentration used *in vitro* was not saturating; Figure 4B), and the concentration of Rnk present *in vivo* was much lower than that of DksA, Rnk therefore is unlikely to compete with DksA for RNAP and affect rRNA promoter activity *in vivo* (see also below).

In contrast, Rnk was only slightly less abundant than GreA and approximately equimolar with GreB in both log and stationary phase (Figure 5A). Equimolar concentrations of Rnk and GreB were sufficient to eliminate GreB function *in vitro* (Figure 4C), and Rnk was able to eliminate GreA function even when GreA was in 5-fold molar excess *in vitro* (Figure 4D). Assuming that the specific activities of the purified proteins are comparable and that the relative affinities of the Gre factors and Rnk for the promoter complex reflect their relative affinities for RNAP

complexes during promoter escape and transcription elongation (where Gre factors are thought to influence transcription), Rnk might be expected to compete with GreB and perhaps even GreA *in vivo*.

To address directly whether Rnk competes with DksA or the Gre factors in cells, we examined the effects of Rnk *in vivo* on transcription from two promoters, the rRNA promoter *rrnB* P1 and the tryptophanase promoter *tnaC*. It was shown previously that DksA negatively regulates *rrnB* P1, and therefore transcription from *rrnB* P1 increases when the *dksA* gene is inactivated [20]. In contrast, Gre factors facilitate promoter escape from *tnaC*, and therefore inactivation of the *gre* genes decreases the activity of this promoter [9].

We measured *rrnB* P1-*lacZ* activity by β-galactosidase assay in a wild-type strain and in a strain deleted for *rnk* (Δ*rnk*). The *rrnB* P1 activity was identical in a wild-type and Δ*rnk* strain in both log and stationary phase (Figure 5B). This result is consistent with the prediction above that Rnk would not compete with DksA for rRNA promoter complexes *in vivo* because Rnk is much less abundant that DksA *in vivo*. However, we have not ruled out that there might be some condition *in vivo* where the two factors are in competition.

Because Rnk and the Gre factors are much closer in concentration *in vivo*, we chose a promoter that had been shown previously to require Gre factor activiy for a more rigorous test of potential competition between Rnk and a secondary channel binding factor *in vivo*. We further increased the chance that the Rnk concentration would be sufficient to compete with the Gre factors by expressing Rnk from an IPTG-inducible promoter (we confirmed that Rnk was greatly overexpressed under these conditions; ~60-fold; Figure 5D).

In aggreement with the previous conclusion that GreA and GreB facilitate escape of RNAP from the *tnaC* promoter [9], we found that the activity of a *tnaC-lacZ* fusion decreased more than 2-fold in a Δ*greA*Δ*greB* strain (Fig. 5C, compare open bars). However, even under these conditions, Rnk did not reduce *tnaC-lacZ* activity; i.e. overexpression of Rnk did not mimic the effect of inactivation of the *gre* genes (Figure 5C). Therefore, we are unable to conclude at this time that the competition between Rnk and the Gre factors observed *in vitro* actually occurs *in vivo*. For unknown reasons, overexpression of Rnk appeared to increase *tnaC* promoter activity very slightly (~1.5-fold) in a Δ*greA*Δ*greB* strain (Figure 5C, right). Clearly, further studies will be needed to determine promoters (if any) where Rnk competes with Gre factors and reduces expression *in vivo*.

Discussion

We report here the structure of Rnk, the relative concentrations of Rnk and GreA, GreB, and DksA (three other factors that bind to the RNAP secondary channel), and the results of competition experiments with these factors performed *in vitro* and *in vivo*. Our results strongly suggest that although Rnk itself appears to have no direct effect on transcription, it shares important RNAP binding determinants with Gre factors, and it binds to RNAP with similar or greater apparent affinity *in vitro*, suggesting that Rnk might inhibit Gre factor function under conditions yet-to-be identified.

The relative orientation of the N-terminal coiled-coil and C-terminal globular domains in the crystal structure of *Ec* GreA was maintained by inter-domain hydrogen bonds involving conserved residues in both of the protein domains [10]. A model of *Taq* Gfh1 suggested that these same residues could also stabilize a GreA-like conformation [23]. This observation was supported by *in vitro* experiments showing the existence of several conformations in solution for Gfh1 [25]. Conserved residues in Rnk, including Asp12, Tyr77 and Glu129, stabilize the Rnk conformation in the Rnk crystal structure. These positions are not conserved in GreA and Gfh1. Rnk Asn9, located at the end of the N-terminal arm, is at the core of the interdomain

hydrogen bond network. Interestingly, *Ec* Rnk Asn9 is replaced by a Thr or Ser in most of the Rnk homologs. It is in the same position as GreA Thr7 and Gfh1 Thr8 involved in similar networks [23].

Mapping sequence similarity from an alignment of 45 Rnk homologs (Figure S1) onto the structure reveals a single cluster of surface-exposed, highly conserved residues (Figure 6A). The cluster contains *Ec* Rnk residues Pro78, Leu88, Ser89, Met91, Pro93, and Gly114. Interestingly, some of the corresponding residues are also conserved and surface-exposed in the Gfh1 and Gre-factors (Figure 1A). Specifically, the residue corresponding to *Ec* Rnk Pro78 is conserved in the Gfh1s, but is a Ser in the Gre-factors. The residue corresponding to *Ec* Rnk Leu88 is highly conserved as a bulky hydrophobic residue among all the factors. Finally, the residues corresponding to *Ec* Rnk Ser89 and Pro93 are strictly conserved among all three families of factors (Rnk, Gfh1, GreA/B). Mutational studies indicate strictly conserved *Ec* GreB Pro123 (corresponding to *Ec* Rnk Pro93) plays a role in RNAP binding [40]. Moreover, the juxtaposition of this surface against the RNAP in the structure-based model of the RNAP/Gre-factor complex is consistent with this region playing a role in the protein/protein complex [13]. These findings suggest that this surface-exposed patch of conserved residues plays a similar functional role (mediating the protein/protein complex with RNAP) among the three families of factors.

We generated Rnk single mutations of P93A, L88A and S89A as well as combination of double mutants and a triple mutant P93A+L88A+S89A to assess their binding to RNAP. Native gel shift analyses failed to show any notable effect of the mutations when compared to wild-type Rnk (data not shown). Considering the highly hydrophobic nature of this surface, it is most likely that multiple interactions contribute to RNAP binding and substitution to alanine might not be drastic enough to disrupt the hydrophobic contacts.

A model of Rnk bound to the TEC (Figure 6B) predicts a minor clash at the extremity of a flexible loop in the Rnk CTD (residues 139 to 150). However this loop displays a wide range of conformations in the structures of Gfh1 and Rnk, and it is completely disordered in *Ec* GreA (Figure S2B), suggesting that this flexible element might be able to adapt to the RNAP surface upon binding. If the Rnk coiled-coil adopts the same relative orientation when bound to RNAP as the *Ec* GreA coiled-coil (Figure 6B), the model predicts that the Rnk coiled-coil would be too short to reach backtracked RNA in the RNAP secondary channel, in agreement with the absence of crosslinking (Figure 3B).

Previous biochemical studies of the Gre factors have shown that truncations of the Gre factors containing only the CTD are still able to competetively bind RNAP with full-length GreA and GreB, thereby inhibiting transcription cleavage activity [12]. Thus, the presence of a long coiled-coil domain is not a pre-requisite for anti-Gre activity. Interactions between the CTD of the Gre factors with the β'G lineage-specific insert in *Ec* have been detected in several studies [14; 41]. The *Taq* and *Tth* anti-Gre factor Gfh1 possesses a coiled-coil of the same length as *Taq* and *Tth* GreA factor. It is possible that additional interactions provided by the *Ec* β'G insert, absent in *Thermus*, compensates for the shorter coiled-coil of its anti-Gre factor Rnk. On the other hand, although only the presence of the CTD is sufficient for inhibiting Gre-stimulated transcript cleavage activity, the presence of a long coiled-coil in *Thermus* anti-Gre Gfh1 might ensure stronger binding and more efficient cleavage inhibition in extreme environmental conditions.

In summary, although we have demonstrated that *Ec* Rnk binds to RNAP and competes *in vitro* with three known secondary channel effectors, GreA, GreB, and DksA, we have been unable as yet to establish the importance of this competition *in vivo*. Likewise, regulation of transcript cleavage activity by *Thermus* anti-Gre factors has also been demonstrated *in vitro*,

but the nutritional/environmental conditions under which this modulation of Gre factor functions *in vivo* remain unclear. Nevertheless, our results suggest that regulation of Gre-stimulated transcript cleavage might be a general feature in transcription that extends beyond hyperthermophilic bacteria.

Materials and Methods

Sequence analysis

Rnk homologs were identified using Ballast (http://bips.ustrasbg.fr/PipeAlign/jump_to.cgi?Ballast+noid) [29]. Sequence alignments were edited using Seqlab and identity percentages were calculated with the identity matrix from the GCG Wisconsin package [42]. Secondary structure predictions were calculated on the web interface with the program PHD (http://npsa-pbil.ibcp.fr/cgi-bin/npsa_automat.pl?page=/NPSA/npsa_phd. html) [30]. The most redundant sequences were removed out of the multiple sequence alignment (identity cutoff 0.95). Six Rnk homologs with large N-terminal insertions were omitted from the final alignment: spt_q73j81, spt_q4kb20, spt_q7w4h3, spt_q5qw19, spt_q3n261 and spt_q8yc75. The resulting sequence alignment (Figure S1) was adjusted manually using Seqlab [42]. The sequences were colored according to their sequence identity conservation using Jalview [43].

The PSI-BLAST search against Swiss-Prot, TRembl and Microbial complete proteomes databases was performed through the website interface (http://myhits.isb-sib.ch/cgi-bin/psi_blast) using Rnk FKBP domain residues 52 to 124 and the BLOSUM-62 matrix (E-value inclusion 1.10^{-3}, E value report 1, clusters matches with approximate level of identity 70%).

Cloning the *rnk* gene

The *rnk* gene was amplified by the polymerase chain reaction (PCR) from *Ec* genomic DNA with primers: ggagtacatatgtccagaccaactatcatcat (forward), gcactcgagttaaagcaggtagtcgccagcag (reverse). The 430 bp DNA fragment was blunt-end cloned into pT7Blue blunt vector (Novagen), and recombinants containing the *rnk* gene in the correct orientation with respect to the T7 promoter were selected.

The *rnk* gene was excised from pT7Blue by NdeI and BamHI restriction endonucleases, and cloned into the pET11a expression vector (Novagen) treated with the same enzymes. To generate Rnk with an N-terminal His_6-tag, the same NdeI-BamHI DNA fragment containing the *rnk* gene was cloned into the pET28a expression vector.

Rnk Purification and Crystallization

The pET11a plasmid producing *Ec* Rnk was transformed into *Ec* BL21(DE3). Colonies were harvested directly from the plates and used to inoculate a 6 L culture. Cells at OD_{600nm}=0.8 were induced with 0.5 mM IPTG for 3 hours at 37°C. The cells were lysed using a French Press in 80 ml of TGED buffer (20 mM Tris-HCl, pH 8.0, 5% glycerol, 0.1 mM EDTA, 1 mM DTT) plus 100 mM NaCl and 0.1 mM PMSF. After 50 min centrifugation at 14000 rpm, the pellet was resuspended in the TGED + 500 mM NaCl and lysed again. The supernatant was recovered after a second centrifugation and protein was precipitated with ammonium sulfate (36% w/v) at 4°C. After centrifugation, the precipitate was dissolved in TGED + 50 mM NaCl and loaded on a 20 ml Q sepharose column (GE Healthcare). The protein was eluted by a gradient from 50 mM to 1 M NaCl over 10 column volumes. Fractions containing Rnk (determined by SDS-PAGE) were pooled and concentrated to 5 ml using a Vivaspin 5000 Da cutoff centrifugal concentrator. The sample was loaded on a Superdex 75 gel filtration column

(GE Healthcare) equilibrated in TGED + 500 mM NaCl. The purified fractions were frozen and stored at −80°C with 15% glycerol.

Individual fractions were dialyzed against 20 mM Tris-HCl, pH 8.0, 50 mM NaCl, 1 mM DTT, and concentrated separately to 9 mg/ml. Crystals grew by vapour diffusion in a couple of days at 22°C in Hampton Natrix Screen condition 1 (50 mM MES, pH 5.6, 10 mM $MgCl_2$, 2.0 M $LiSO_4$). Microseeding was used to obtain large single crystals, with the final well conditions being refined to 50 mM MES, pH 5.6, 10 mM $MgCl_2$, 1.5 M $LiSO_4$. For cryocrystallography, the crystals were dunked in a cryosolution containing only 2.5 M $LiSO_4$ and frozen in liquid ethane.

Structure determination

Frozen Rnk crystals diffracted beyond 2 Å-resolution on an X-ray home source. A native dataset was collected to 2 Å-resolution at NSLS beamline X9A (Table 1). A highly redundant dataset (Sulfur, Table 1) was collected from a single crystal at the iron edge to observe the sulfur anomalous signal from the native protein. The data were analyzed using XPREP [44]. Phasing was performed with SOLVE [45] between 20 and 1.91 Å using the sulfur sites found with SHELX [44; 46]. Out of the 18 anomalous sites found by SHELX, 4 were sulfate ions bound at the surface of the protein, and 2 were chloride ions. Density modification performed with DM using non-crystallographic two-fold symmetry [47] yielded a very clear map and most of the main chain was built with ArpWarp [48]. Loops and side chains were built manually in O. The structure was refined to 1.91 Å using CNS [49] with the anomalous data processed with Scalepack [50]. The final model (R=21.2%, Rfree=23.7 %) consists of two copies of Rnk, 282 water molecules, 10 sulfate ions, and 2 chloride ions. PROCHECK [51] revealed no residues in the disallowed regions of the Ramachandran plot.

Biochemical Assays

Ni^{2+}-NTA agarose binding assay—Binding reactions (50 µl) contained approximately 5 pmol of core RNAP plus 75 pmol of His_6-Rnk (Figure 3A, lanes 1–4) or no Rnk (Figure 3A, lanes 5–8) in binding buffer (20 mM Tris-HCl, pH 7.9, 125 mM NaCl, 0.5 mM imidazole). Reactions were incubated for 10 min. at room temperature, then added to 15 µl of Ni^{2+}-NTA agarose beads (Qiagen; pre-equilibrated with binding buffer) and further incubated for 10 min. at room temperature with gentle mixing of the beads. The beads were pelleted by brief centrifugation, and unbound material in the supernatant was withdrawn. The beads were then washed three times with 1 ml of binding buffer, then eluted with 30 µl binding buffer + 100 mM imidazole. The protein samples were precipitated with 7% trichloroacetic acid and analyzed by SDS-PAGE (Figure 3A).

TEC preparation—All TECs were prepared by using a PCR-amplified 202-bp DNA fragment (−152 to +50 bp) containing the *Ec* rrnB P1 promoter [1; 52]. TECs containing a 6-nt transcript (TEC6=CpApCpCpApC) were prepared by incubating 7.3 pmol of the promoter DNA fragment for 10 min at 37°C with 30 pmol of RNAP, BSA (1 mg/ml), 1 mM CpA, 10 µM ATP, and 1 µM [α-^{32}P]CTP (3000 Ci/mmol) in 35 µL of transcription buffer (40 mM Tris acetate, pH 7.9, 30 mM KCI, 10 mM $MgCl_2$). TECs containing a 9-nt transcript (TEC9=CpApCpCpApCpUpGpA) were obtained by chain extension of unlabelled TEC6 with 10 µM UTP, 10 µM ATP, and 1 µM [α-^{32}P]GTP (3000 Ci/mmol) for 5 min at 37°C. TEC9 containing 8-N_3(azido)AMP at the RNA 3'-terminus was obtained by chain extension of TEC6 with 10 µM UTP, 100 µM 8-N_3-ATP, and 1 µM [α-^{32}P]GTP (3000 Ci/mmol) for 5 min at 37°C. The complexes were purified by gel filtration on Quick-Spin G-50 columns in 10 mM Tris-HCl, pH 8.0, 1 mM EDTA.

Competetive crosslinking assay—Combinations of Rnk and GreA (as specified in Figure 3B) were added to TEC9 containing 8-N_3-AMP at the RNA 3'-terminus, and incubated for 10 min at 37°C. Photocrosslinking was performed by UV-radiation at 310 nm for 20 min on ice [10]. Reactions were terminated by the addition of an equal volume of SDS gel-loading buffer (2x) and analyzed by Tris-Tricine SDS-16%-PAGE followed by autoradiography and quantification by PhosphorImagery.

Transcript cleavage reactions—Reactions were performed in 10 μl of transcription buffer containing 2.5 nM TEC6 or TEC9 and other factors as specified (Figure 3C; nothing, Mg^{2+}, GreA, GreB, or Rnk) for 10 min at 37°C. After incubation, 10 μl of formamide buffer was added, and the samples were analyzed by urea-23%-PAGE, visualized by autoradiography, and quantified using a PhosphorImager.

RNAP-promoter complex decay assays—RNAP-promoter complex decay assays were performed as described [21]. Half-lives of RNAP-promoter complexes (Figure 4) were determined using a filter-binding assay [53]. Briefly, approximately 0.2 nM of a 242 bp XhoI restriction fragment containing the *lacUV5* promoter (*lac* sequence endpoints −60 to +40) from pRLG4264 was ^{32}P end-labeled and incubated with 10 nM RNAP in transcription buffer (40 mM Tris HCl pH 7.9, 10 mM $MgCl_2$, 1 mM DTT, 0.1 mg/ml BSA) containing 100 mM NaCl and the concentration of Rnk, DksA, GreB, GreA, or storage buffer indicated (Figure 4 legend) at 30 ° C for 20 min. Heparin (to 10 μg/ml) was added, aliquots were removed at the indicated times, and RNAP-promoter complexes were captured on nitrocellulose filters. The radioactivity retained was determined by phosphorimaging, and half-lives were calculated as described [53].

Promoter activity measurements in vivo—Construction of promoter-*lacZ* fusions on monolysogens of phage λ and β-galactosidase assays were performed as described [21]. Briefly, promoter fusions were created by *in vitro* ligation of an *rrnB* P1 promoter fragment (endpoints −66 to +9 with respect to the transcription start site) to purified phage DNA arms containing the *lacZ* gene, followed by phage packaging and infection, or by *in vivo* recombination of a *tnaC* promoter (endpoints −189 to +21) into phage λ DNA carrying *lacZ*. Strains containing or lacking the *rnk* gene or the *greA* and *greB* genes were grown in LB for ~4 generations to an OD_{600} of ~0.4 (for log phase) or for ~24 hr to an OD_{600} of ~5.0 (stationary phase). Where indicated, cells carried an empty plasmid vector, pINIIIA1 (RLG6332), or a plasmid expressing Rnk from the IPTG-inducible *lpp-lac* promoter, pRnk (pRLG9163), and were grown in the presence of 100 μg/ml ampicillin. pRnk was constructed by cloning the *rnk* coding region (from 19 bp upstream of the AUG to 29 bp downstream of the stop codon) into pINIIIA1 (pRLG6332) between the XbaI and HindIII sites, as described [20]. Cells were harvested, chilled on ice for ~20 min, lysed by sonication, and β-galactosidase activity was determined by standard methods [53]. The *greA* and *greB* deletions were as described [21]. The *rnk* strain (Δ*rnk*) was generously provided by K. Datsenko and B. Wanner (Purdue University) and was constructed using Red-mediated recombination as described previously [9; 54]. Details are available on request.

Quantitative Western blots—Western blots were performed as described [21]. Protein concentrations were determined from 50–100 ml cultures grown in a MOPS-based minimal medium containing 0.4% glycerol, 40 μg/ml each of tryptophan and tyrosine, and 80 μg/ml each of the other 18 amino acids at 30°C and from the LB cultures used for β-galactosidase assays. After growth to the indicated optical densities (see above) and 20 min on ice, cells were harvested by centrifugation, suspended in ≤1 ml of 10 mM Tris-HCl, pH 7.9, 1 mM EDTA, 5% glycerol, 0.1 mM PMSF, lysed by sonication, and centrifuged to remove insoluble material. The total soluble protein concentration was determined with Bradford Assay Reagent using

BSA as a standard. A range of purified DksA, GreA, GreB, and Rnk concentrations was used to construct standard curves. Lysates and standards were separated on 4–12% SDS-polyacrylamide gels (Invitrogen), transferred electrophoretically to PVDF membranes (Bio-Rad), and Western blots were performed as described [20]. For detection of DksA, GreA, GreB, and Rnk, ~5 μg, ~40 μg, ~100 μg, and ~50 μg protein lysate were used, respectively. Rabbit polyclonal anti-DksA antiserum was a generous gift from D. Downs (UW-Madison) and was precleared with total lysate from a strain lacking *dksA*. Mouse monoclonal anti-GreA, anti-GreB, and anti-Rnk antisera were produced by NeoClone, Inc (Madison, WI). An HRP-conjugated secondary antibody (specific to rabbit IgG for polyclonal or to mouse IgG for monoclonal antibodies; Santa Cruz Biotechnology) was detected using ECL+ reagent (GE Healthcare). Western blots were scanned with a Typhoon phosphorimager [GE Healthcare, 520 BP 40 Cy2, ECL+ Blue family (emission), ECL+ excitation (laser)], quantified with ImageQuant (Molecular Dynamics), and protein amounts in the cell lysates were interpolated from the standard curve.

Supplementary Material

Refer to Web version on PubMed Central for supplementary material.

Acknowledgements

We thank K. Datsenko and B. Wanner for making the *rnk* mutant strain available in advance of publication and C. Villers for technical assistance. Figures were generated with DINO (http://www. dino3d.org). National Institutes of Health (GM37048 to R.L.G., GM59295 to K.S., and GM61898 to S.A.D.); University of Wisconsin (University of Wisconsin Distinguished Graduate Student Research Fellowship to S.T.R.).

References

1. Borukhov S, Sagitov V, Goldfarb A. Transcript cleavage factors from *E. coli*. Cell 1993;72:459–466. [PubMed: 8431948]
2. Fish RN, Kane CM. Promoting elongation with transcript cleavage stimulatory factors. Biochim. Biophys. Acta 2002;1577:287–307. [PubMed: 12213659]
3. Marr MT, Roberts JW. Function of transcription cleavage factors GreA and GreB at a regulatory pause site. Mol. Cell 2000;6:1275–1285. [PubMed: 11163202]
4. Toulme F, Mosrin-Huaman C, Sparkowski J, Das A, Leng M, Rahmouni AR. GreA and GreB proteins revive backtracked RNA polymerase in vivo by promoting transcript trimming. EMBO J 2000;19:6853–6859. [PubMed: 11118220]
5. Borukhov S, Lee J, Laptenko O. Bacterial transcription elongation factors: new insights into molecular mechanism of action. Mol Microbiol 2005;55:1315–1324. [PubMed: 15720542]
6. Erie DA, Hajiseyedjavadi O, Young MC, von Hippel PH. Multiple RNA polymerase conformations and GreA: control of the fidelity of transcription. Science 1993;262:867–873. [PubMed: 8235608]
7. Hochschild A. Gene-specific regulation by a transcript cleavage factor: facilitating promoter escape. J. Bacteriol 2007;189:8769–8771. [PubMed: 17951384]
8. Hsu LH, Vo NV, Chamberlin MJ. *Escherichia coli* transcript cleavage factors GreA and GreB stimulate promoter escape and gene expression *in vivo* and *in vitro*. Proc. Natl. Acad. Sci. USA 1995;92:11588–11592. [PubMed: 8524809]
9. Stepanova E, Lee J, Ozerova M, Semenova E, Datsenko K, Wanner BL, Severinov K, Borukhov S. Analysis of promoter targets for Escherichia coli transcription elongation factor GreA in vivo and in vitro. J. Bacteriol 2007;189:8772–8785. [PubMed: 17766423]
10. Stebbins CE, Borukhov S, Orlova M, Polyakov A, Goldfarb A, Darst SA. Crystal structure of the GreA transcript cleavage factor from *Escherichia coli*. Nature 1995;373:636–640. [PubMed: 7854424]

11. Koulich D, Orlova M, Malhotra A, Sali A, Darst SA, Goldfarb A, Borukhov S. Domain organization of transcript cleavage factors GreA and GreB. J. Biol. Chem 1997;272:7201–7210. [PubMed: 9054416]
12. Koulich D, Nikiforov V, Borukhov S. Distinct functions of N- and C-terminal domains of GreA, an *Escherichia coli* transcript cleavage factor. J. Mol. Biol 1998;276:379–389. [PubMed: 9512710]
13. Opalka N, Chlenov M, Chacon P, Rice WJ, Wriggers W, Darst SA. Structure and function of the transcription elongation factor GreB bound to bacterial RNA polymerase. Cell 2003;114:335–345. [PubMed: 12914698]
14. Laptenko O, Lee J, Lomakin I, Borukhov S. Transcript cleavage factors GreA and GreB act as transient catalytic components of RNA polymerase. EMBO J 2003;23:6322–6334. [PubMed: 14633991]
15. Sosunov V, Sosunova E, Mustaev A, Bass I, Nikiforov V, Goldfarb A. Unified two-metal mechanism of RNA synthesis and degradation by RNA polymerase. EMBO J 2003;22:2234–2244. [PubMed: 12727889]
16. Sosunova E, Sosunov V, Kozlov M, Nikiforov V, Goldfarb A, Mustaev A. Donation of catalytic residues to RNA polymerase active center by transcription factor Gre. Proc. Natl. Acad. Sci. USA. 2003in press
17. Perederina A, Svetlov V, Vassylyeva M, Tahirov T, Yokoyama S, Artsimovitch I, Vassylyev D. Regulation through the secondary channel - structural framework for ppGpp-DksA synergism during transcription. Cell 2004;118:297–309. [PubMed: 15294156]
18. Nickels BE, Hochschild A. Regulation of RNA polymerase through the secondary channel. Cell 2004;118:281–284. [PubMed: 15294154]
19. Paul BJ, Berkmen MB, Gourse RL. DksA potentiates direct activation of amino acid promoters by ppGpp. Proc. Natl. Acad. Sci. USA 2005;102:7823–7828. [PubMed: 15899978]
20. Paul BJ, Barker M, Ross W, Schneider D, Webb C, Foster J, Gourse R. DksA: A critical component of the transcription intiiation machinery that potentiates the regulation of rRNA promoters by ppGpp and the initiating NTP. Cell 2004;118:311–322. [PubMed: 15294157]
21. Rutherford ST, Lemke JJ, Vrentas CE, Gaal T, Ross W, Gourse RL. Effects of DksA, GreA, and GreB on transcription initiation: insights into the mechanisms of factors that bind in the secondary channel of RNA polymerase. J Mol Biol 2007;366:1243–1257. [PubMed: 17207814]
22. Hogan BP, Hartsch T, Erie DA. Transcript cleavage by *Thermus thermophilus* RNA polymerase. Effects of GreA and anti-GreA factors. J. Biol. Chem 2002;277:967–975. [PubMed: 11606592]
23. Lamour V, Hogan BP, Erie DA, Darst SA. Crystal structure of Thermus aquaticus Gfh1, a Gre-factor homolog that inhibits rather than stimulates transcript cleavage. J. Mol. Biol 2006;356:179–188. [PubMed: 16337964]
24. Symersky J, Perederina A, Vassylyeva MN, Svetlov V, Artsimovitch I, Vassylyev DG. Regulation through the RNA polymerase secondary channel. Structural and functional variability of the coiled-coil transcription factors. J Biol Chem 2006;281:1309–1312. [PubMed: 16298991]
25. Laptenko O, Kim SS, Lee J, Starodubtseva M, Cava F, Berenguer J, Kong XP, Borukhov S. pH-dependent conformational switch activates the inhibitor of transcription elongation. Embo J 2006;25:2131–2141. [PubMed: 16628221]
26. Shankar S, Schlictman D, Chakrabarty AM. Regulation of nucleoside diphosphate kinase and an alternative kinase in Escherichia coli: role of the sspA and rnk genes in nucleoside triphosphate formation. Mol Microbiol 1995;17:935–943. [PubMed: 8596442]
27. Schlictman D, Shankar S, Chakrabarty AM. The Escherichia coli genes sspA and rnk can functionally replace the Pseudomonas aeruginosa alginate regulatory gene algR2. Mol Microbiol 1995;16:309–320. [PubMed: 7565093]
28. Van Duyne GD, Standaert RF, Karplus PA, Schreiber SL, Clardy J. Atomic structure of FKBP-FK506, an immunophilin-immunosuppressant complex. Science 1991;252:839–842. [PubMed: 1709302]
29. Plewniak F, Thompson JD, Poch O. Ballast: blast post-processing based on locally conserved segments. Bioinformatics 2000;16:750–759. [PubMed: 11108697]
30. Rost B, Sander C. Prediction of protein structure at better than 70% accuracy. J. Mol. Biol 1993;232:584–599. [PubMed: 8345525]
31. Sekerina E, Rahfeld JU, Muller J, Fanghanel J, Rascher C, Fischer G, Bayer P. NMR solution structure of hPar14 reveals similarity to the peptidyl prolyl cis/trans isomerase domain of the mitotic regulator

hPin1 but indicates a different functionality of the protein. J Mol Biol 2000;301:1003–1017. [PubMed: 10966801]

32. Van Duyne GD, Standaert RF, Karplus PA, Schreiber SL, Clardy J. Atomic structures of the human immunophilin FKBP-12 complexes with FK506 and rapamycin. J Mol Biol 1993;229:105–124. [PubMed: 7678431]
33. Vogtherr M, Jacobs DM, Parac TN, Maurer M, Pahl A, Saxena K, Ruterjans H, Griesinger C, Fiebig KM. NMR solution structure and dynamics of the peptidyl-prolyl cis-trans isomerase domain of the trigger factor from Mycoplasma genitalium compared to FK506-binding protein. J Mol Biol 2002;318:1097–1115. [PubMed: 12054805]
34. Riboldi-Tunnicliffe A, Konig B, Jessen S, Weiss MS, Rahfeld J, Hacker J, Fischer G, Hilgenfeld R. Crystal structure of Mip, a prolylisomerase from Legionella pneumophila. Nat Struct Biol 2001;8:779–783. [PubMed: 11524681]
35. Gupta A, Kumar PH, Dineshkumar TK, Varshney U, Subramanya HS. Crystal structure of Rv2118c: an AdoMet-dependent methyltransferase from Mycobacterium tuberculosis H37Rv. J Mol Biol 2001;312:381–391. [PubMed: 11554794]
36. Sinars CR, Cheung-Flynn J, Rimerman RA, Scammell JG, Smith DF, Clardy J. Structure of the large FK506-binding protein FKBP51, an Hsp90-binding protein and a component of steroid receptor complexes. Proc Natl Acad Sci U S A 2003;100:868–873. [PubMed: 12538866]
37. Bitto E, McKay DB. Crystallographic structure of SurA, a molecular chaperone that facilitates folding of outer membrane porins. Structure 2002;10:1489–1498. [PubMed: 12429090]
38. Altschul SF, Madden TL, Schaffer AA, Zhang J, Zhang Z, Miller W, Lipman DJ. Gapped BLAST and PSI-BLAST: a new generation of protein database search programs. Nucleic Acids Res 1997;25:3389–3402. [PubMed: 9254694]
39. Sen R, Nagai H, Shimamoto N. Conformational switching of Escherichia coli RNA polymerase-promoter binary complex is facilitated by elongation factor GreA and GreB. Genes Cells 2001;6:389–401. [PubMed: 11380617]
40. Loizos N, Darst SA. Mapping interactions of *Escherichia coli* GreB with NA polymerase and ternary elongation complexes. J. Biol. Chem 1999;274:23378–23386. [PubMed: 10438515]
41. Zakharova N, Bass I, Arsenieva E, Nikiforov V, Severinov K. Mutations in and monoclonal antibody binding to evolutionary hypervariable region of *E. coli* RNA polymerase β' subunit inhibit transcript cleavage and transcript elongation. J. Biol. Chem 1998;273:19371–19374. [PubMed: 9677352]
42. Womble DD. GCG: The Wisconsin Package of sequence analysis programs. Methods Mol Biol 2000;132:3–22. [PubMed: 10547828]
43. Clamp M, Cuff J, Searle SM, Barton GJ. The Jalview Java alignment editor. Bioinformatics 2004;20:426–427. [PubMed: 14960472]
44. Uson I, Sheldrick GM. Advances in direct methods for protein crystallography. Curr Opin Struct Biol 1999;9:643–648. [PubMed: 10508770]
45. Terwilliger TC, Berendzen J. Automated MAD and MIR structure solution. Acta Crystallogr. D Biol. Crystallogr 1999;D55:849–861. [PubMed: 10089316]
46. Schneider TR, Sheldrick GM. Substructure solution with SHELXD. Acta Crystallogr D Biol Crystallogr 2002;58:1772–1779. [PubMed: 12351820]
47. Cowtan K. Dm-density modification package. ESF/CCP4 Newsletter 1994;31:34–38.
48. Perrakis A, Morris R, Lamzin VS. Automated protein model building combined with iterative structure refinement. Nature Struct. Biol 1999;6:458–463. [PubMed: 10331874]
49. Adams PD, Pannu NS, Read RJ, Brunger AT. Cross-validated maximum likelihood enhances crystallographic simulated annealing refinement. Proc. Natl. Acad. Sci. USA 1997;94:5018–5023. [PubMed: 9144182]
50. Otwinowski Z, Minor W. Processing of X-ray diffraction data collected in oscillation mode. Methods Enzymol 1997;276:307–326.
51. Laskowski RA, MacArthur MW, Moss DS, Thornton JM. PROCHECK - A program to check the stereochemical quality of protein structures. J. appl. Crystallogr 1993;26:283–291.
52. Borukhov S, Polyakov A, Nikiforov V, Goldfarb A. GreA protein: A transcription elongation factor from *Escherichia coli*. Proc. Natl. Acad. Sci. USA 1992;89:8899–8902. [PubMed: 1384037]

53. Barker MM, Gaal T, Josaitis CA, Gourse RL. Mechanism of regulation of transcription intiiation by ppGpp. I. Effects of ppGpp on transcription initiaiton in vivo and in vitro. J. Mol. Biol 2001;305:673–688. [PubMed: 11162084]

54. Datsenko KA, Wanner BL. One-step inactivation of chromosomal genes in Escherichia coli K-12 using PCR products. Proc. Natl. Acad. Sci. USA 2000;97:6640–6645. [PubMed: 10829079]

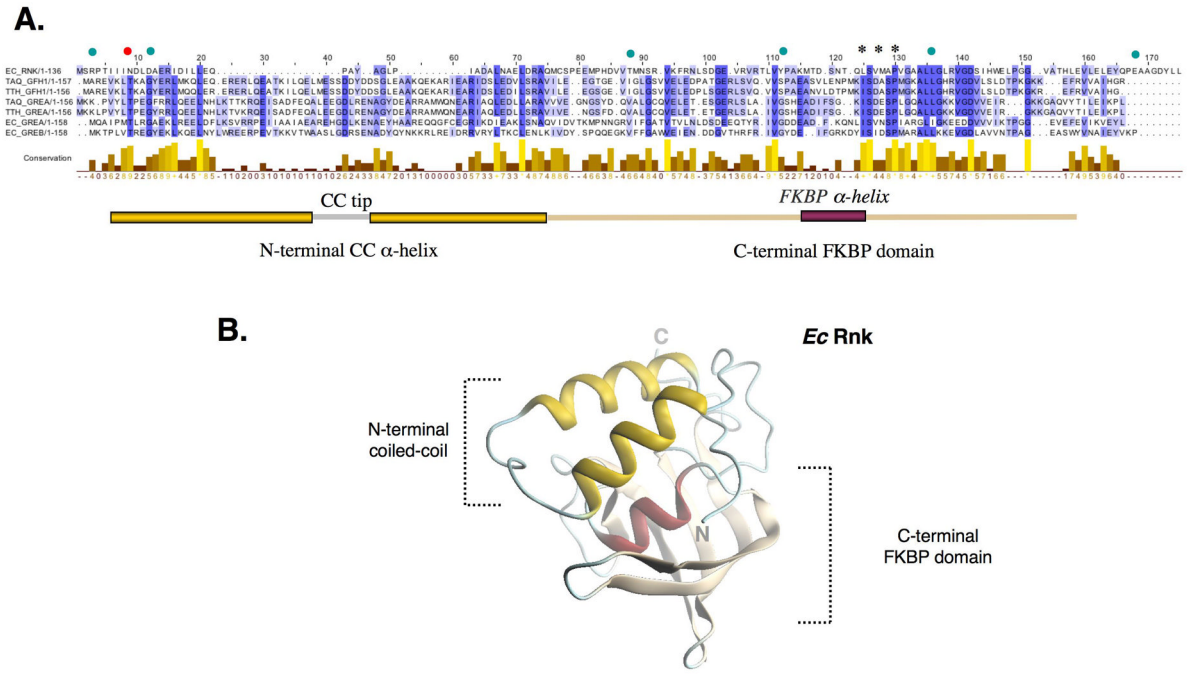

Figure 1. *Ec* Rnk is a Gre-factor/Gfh1 homolog

(**A**) Primary sequence alignment of Rnk with selected Gre and anti-Gre factors. Residues are shaded according to their sequence conservation using the program Jalview [43]. Limits of the NTD and CTD are indicated below the sequences. Stars above the sequences mark conserved residues in the FKBP domain part of a flat hydrophobic surface around Pro93, a residue involved in RNAP binding in Gre factors [40]. Green dots indicate residues involved in Rnk inter-domain interactions. The red dot indicates a position involved in the stabilization of Gre and anti-Gre conformation observed so far in all known structures of Gre factors.

(**B**) The *Ec* Rnk crystal structure is displayed in ribbon representation. The N-terminal coiled-coil appears in yellow, the FKBP domain is made of a β-sheet (beige) flanked by a small α-helix (red).

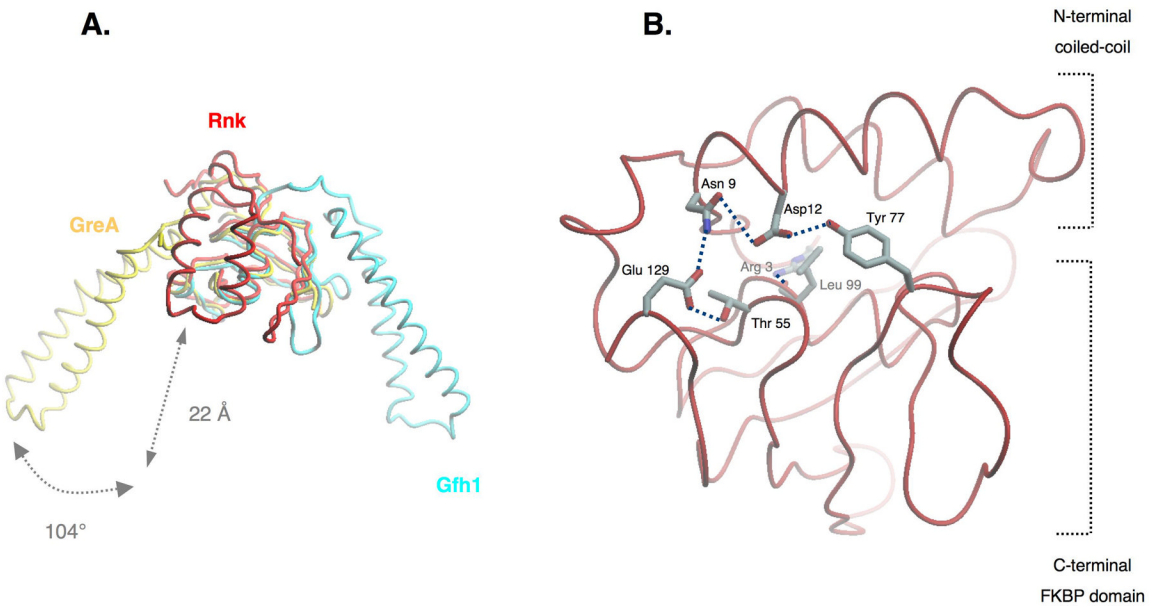

Figure 2. Rnk interdomain orientation

(**A**) *Ec* Rnk (red) superposition with *Ec* GreA (yellow; 10 and *Taq* Gfh1 [23]. The structures have been superimposed on the C-terminal FKBP domain. The Rnk coiled-coil is rotated 104° away from the coiled-coil position observed in *Ec* GreA. The Rnk coiled-coil is 22 Å shorter than the GreA and Gfh1 coiled-coils.

(**B**) *Ec* Rnk interdomain hydrogen bond network. Side chains of N-terminal residues Arg3, Asn9, and Asp12 interact with amino-acids Thr55, Tyr77, Leu99, and Glu129 of the C-terminal FKBP domain.

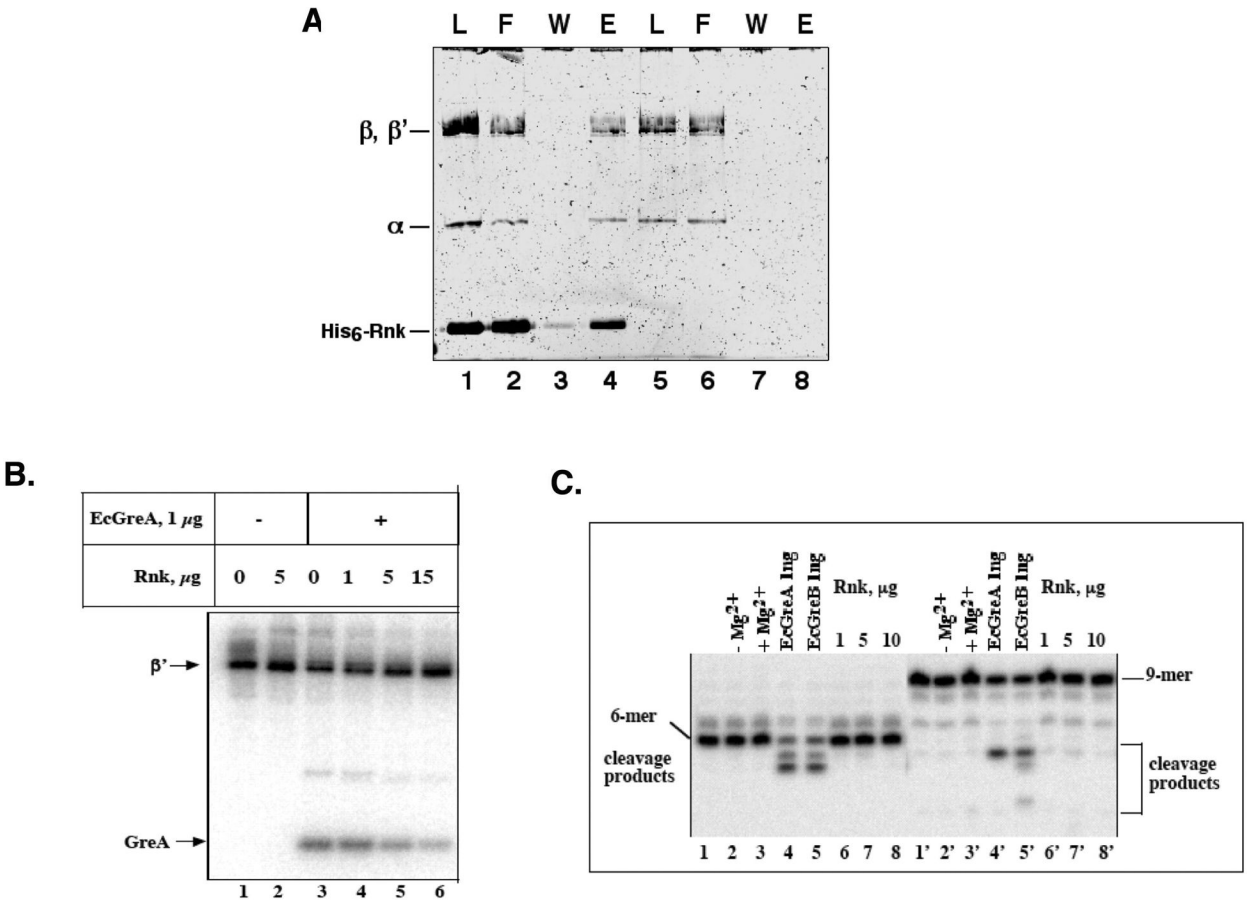

Figure 3. Rnk binds RNAP competitively with Gre-factors

(**A**) Binding of core RNAP to Ni^{2+}-NTA immobilized His_6-Rnk. His_6-Rnk and a molar excess of core RNAP (Load, lane 1) were incubated with Ni^{2+}-NTA agarose beads in buffer containing 0.5 mM imidazole. The beads were washed with buffer containing 0.5 mM imidazole (Flow-throuth, lane 2), then washed with buffer containing 10 mM imidazole (Wash, lane 3), then eluted with buffer containing 100 mM imidazole (Elution, lane 4). The presence of core RNAP in the Elution (lane 4) indicates binding. A separate control experiment shows that core RNAP was not immobilized in the absence of His_6-Rnk (lanes 5–8).

(**B**) Functional (RNA 3'-end crosslinking) competition of Rnk with Gre-factors. TECs with crosslinkable 8-N_3-AMP incorporated in the 3'-end of the 9mer RNA transcript were prepared and crosslinked with GreA in the presence of increasing amounts of Rnk (lanes 3 to 6). The presence of Rnk decreases GreA crosslinking to the RNA.

(**C**) Rnk lacks transcript cleavage activity. TECs containing 6 (lanes 1–8) and 9 (lanes 1'–8') nt-long nascent RNAs were prepared on the rrnB P1 promoter and incubated with Gre-factors or Rnk in the presence of Mg^{2+}.

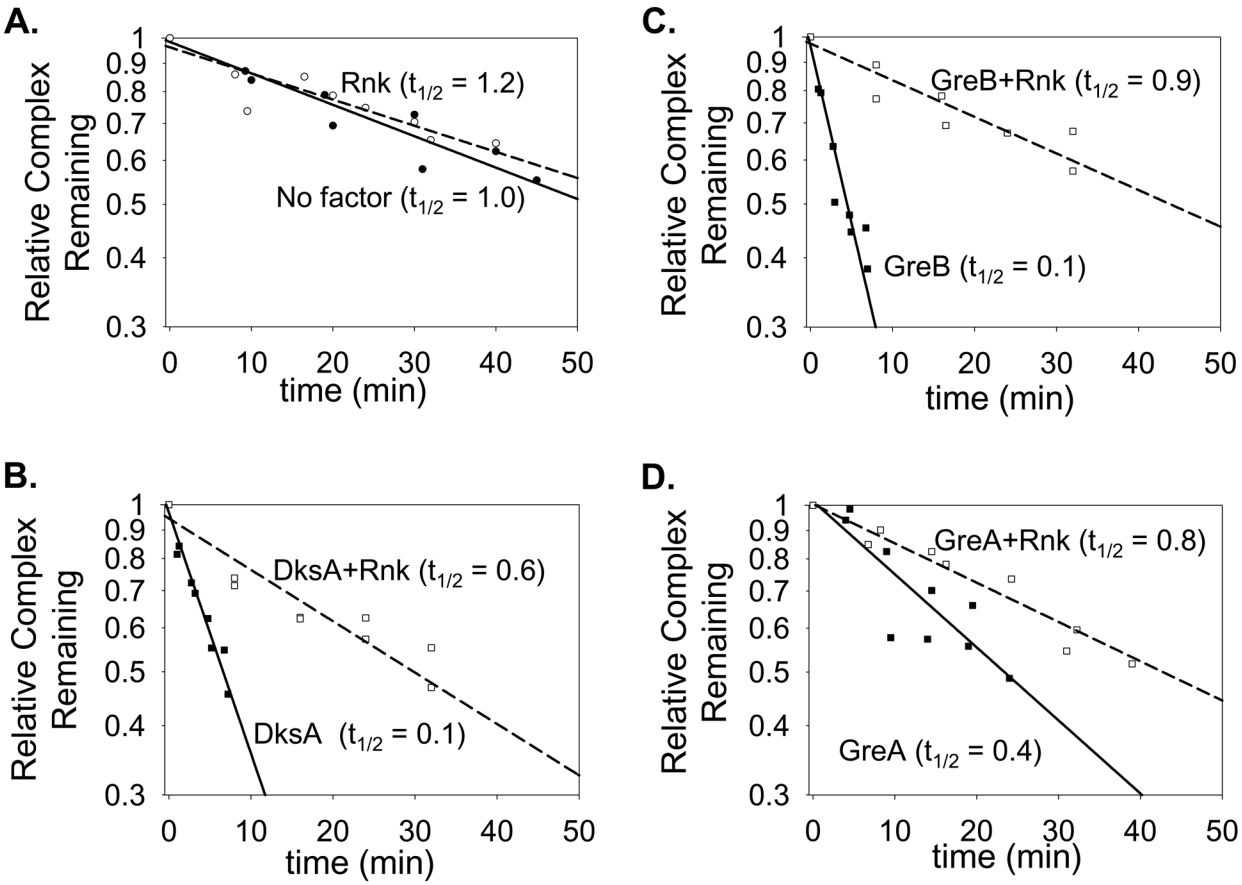

Figure 4. Functional (reduction of open promoter complex half-life) competition of Rnk with secondary channel effectors

The half-life of the RNAP-*lacUV5* competitor-resistant complex was determined in the absence (filled symbols, solid lines) and presence (open symbols, dashed lines) of 0.5 μM Rnk with (**A**) buffer (circles), (**B**) 0.5 μM DksA (squares), (**C**) 0.5 μM GreB (diamonds), or (**D**) 2.5 μM GreA (triangles) using a filter binding assay (see Materials and Methods). The decay curves show the fraction of complexes remaining versus time after heparin addition. Curves for the lifetimes without factors ($t_{1/2}$ ratio = 1.0) are shown in each panel for comparison. Although the curves are displayed in separate panels for clarity, all were carried out at the same time under the same conditions. Thus, the absolute half-lives can be compared directly. The value provided in parenthesis ($t_{1/2}$ ratio) for each curve is the half-life of the competitor-resistant complex relative to that of the same complex in the absence of factor.

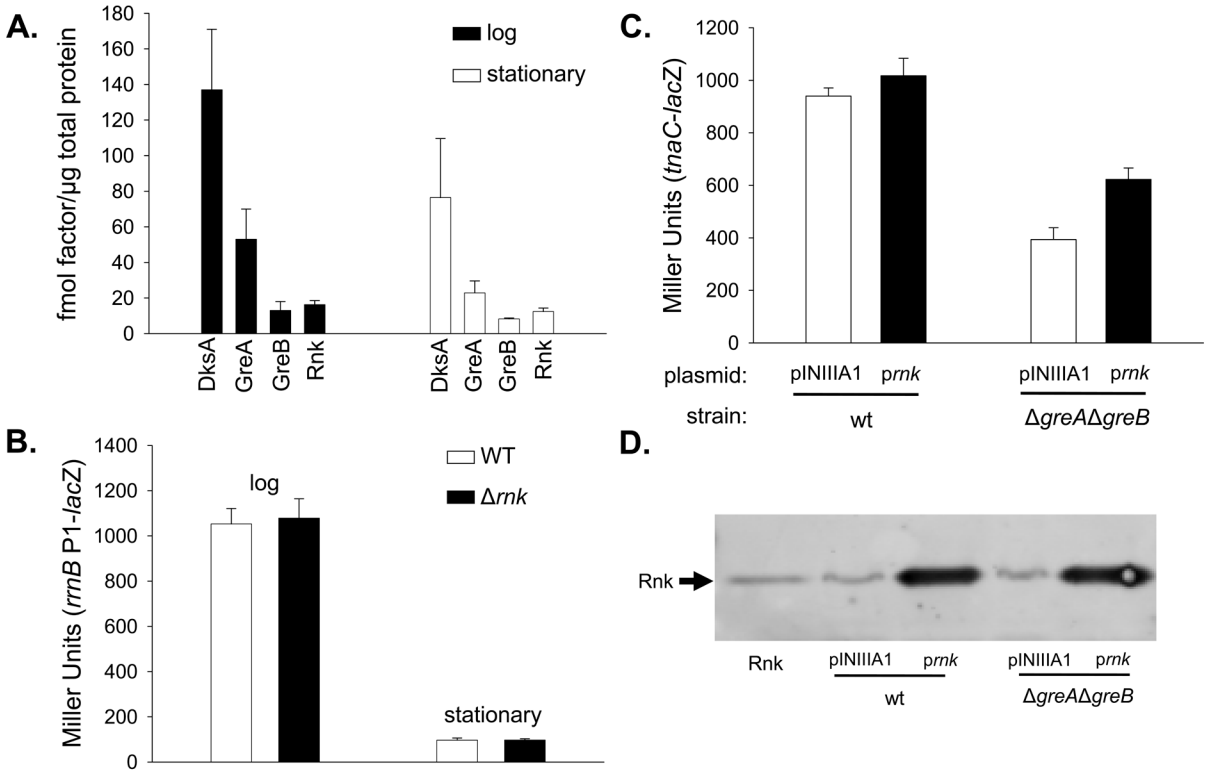

Figure 5. Cellular levels of Rnk are insufficient to affect DksA function, but are similar to levels of GreB

(**A**) The *in vivo* concentration of Rnk is lower than DksA and GreA, but comparable to GreB in log and stationary phase. Quantitative Western blots were performed on cell lysates of a wild-type strain (RLG5950) grown in MOPS medium (see Materials and Methods) in log phase (OD600~0.4) and stationary phase (OD600>4.5). Concentrations (fmol factor/µg total protein) were determined from at least 3 separate experiments (except for Rnk in stationary phase which was determined from 2 experiments).

(B) The *rnk* gene is dispensable for rRNA regulation *in vivo*. β-galactosidase activities (expressed in Miller Units) were determined in strains containing *lacZ* fused to *rrnB* P1. Promoter activities were assayed in wild-type (RLG3739) and Δ*rnk* (RLG8255) cells growing in LB at 30°C in log phase (OD600~0.4 after ~4 generations of growth) and stationary phase (24 hr). β-galactosidase activities from ≥4 cultures were averaged and standard errors are shown.

(**C**). Rnk does not inhibit Gre factor function in *tnaC* expression *in vivo*. β-galactosidase activities (expressed in Miller Units) were determined in strains containing *lacZ* fused to the *tnaC* promoter region. Promoter activities were assayed in wild-type (RLG9166) and Δ*greA*Δ*greB* (RLG9168) cells carrying an empty vector, pINIIIA1 (pRLG6332), or a vector expressing Rnk from the IPTG-inducible *lpp-lac* promoter, pRnk (pRLG9163). Cells were grown in LB at 30°C with 100 µg/ml ampicillin and 1 mM IPTG, and β-galactosidase activity was assayed in log phase (OD600~0.4 after ~4 generations of growth). β-galactosidase activities from ≥4 cultures were averaged and standard errors are shown. Similar trends were observed in stationary phase (date not shown)

(**D**). Rnk was overexpressed from the IPTG inducible *lpp-lac* promoter. Rnk levels were measured by Western blots performed on cell lysates from the cultures assayed for β-galactosidase activity described above. 40 ng of purified Rnk, ~39 µg of total protein from the cultures carrying the empty vector, pINIIIA1 (pRLG6332), and ~7.8 µg of total protein from

the cultures carrying p*rnk* (pRLG9163) were probed with anti-Rnk antibody. A representative blot is shown. Similar results were observed in stationary phase (data not shown).

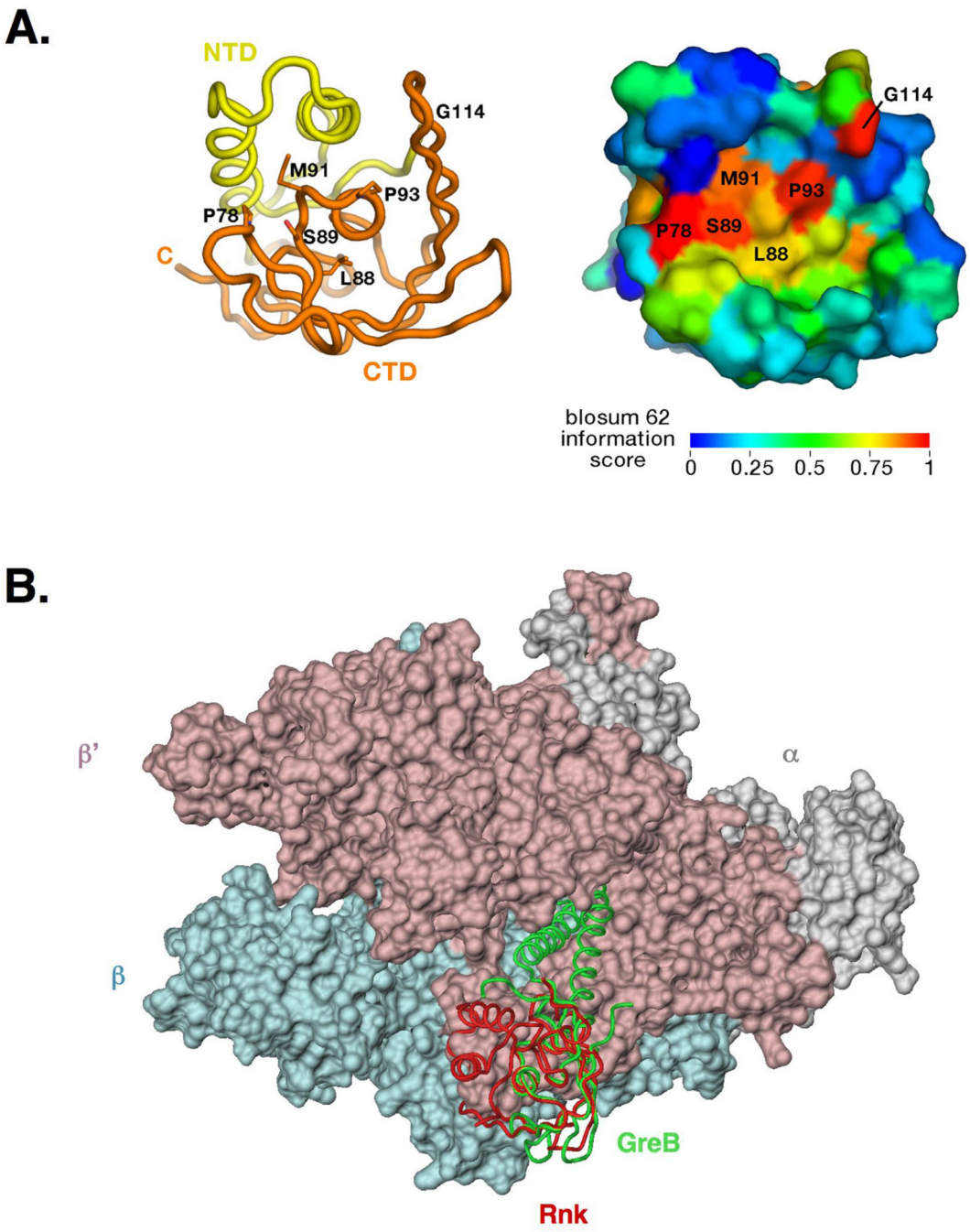

Figure 6. Potential RNAP binding surface of Rnk

(**A**). Rnk C-terminal FKBP domain conserved residues. (left) Conserved residues in the Rnk family (see alignment Figure S1) are highlighted on the RNK structure (worm representation with NTD in yellow and FKBP domain in orange) and (right) in a molecular surface representation colored according to the BLOSUM score.

(**B**). RNAP model with Rnk (red backbone worm) and GreB (green backbone worm) C-terminal FKBP domains superposed [13].

Table 1

Crystallographic Analysis

Diffraction data

Data set	Wavelength (Å)	Resolution (Å)	Number of reflections (Total/ Unique)	Completeness	I/σ	R_{sym} [a] (%)	Redundancy	No. of sites
Sulfur	1.74326	20-1.91 (1.98-1.91)	787,643/44,841	98.8 (97.5)	57.3 (13.7)	6.2 (23.3)	17.2	18

Crystal space group	C2221
Unit cell	a = 68.46 Å, b = 133.39 Å, c = 66.02 Å
Solvent content	55.85 % (2 molecules in the asymmetric unit)
Figure of Merit[b] (30-2.3 Å)	0.25

Refinement

Resolution	20.0 - 1.91 Å
R_{cryst} / R_{free} [c] (%)	21.2 / 23.7 %
rmsd bonds	0.006 Å
rmsd angles	1.40°

The final model contains 270 residues, 282 water molecules, 10 sulfates ions, 2 chloride ions

[a] Rsym = Σ|I-<I>|/ΣI, where I is observed intensity and <I> is average intensity obtained from multiple observations of symmetry-related reflections.

[b] Figure of merit as calculated by SOLVE [45].

[c] $R_{cryst} = \Sigma||F_{observed}|-|F_{calculated}||/\Sigma|F_{observed}|$, $R_{free} = R_{cryst}$ calculated using 9.3% random data omitted from the refinement.